IAI
Journals.ASM.org

Critical Roles of Notch and Wnt/β-Catenin Pathways in the Regulation of Hyperplasia and/or Colitis in Response to Bacterial Infection

Ishfaq Ahmed,[a] Parthasarathy Chandrakesan,[b] Ossama Tawfik,[c] Lijun Xia,[d] Shrikant Anant,[a] and Shahid Umar[a]

Departments of Molecular and Integrative Physiology[a] and Anatomic and Surgical Pathology,[c] University of Kansas Medical Center, Kansas City, Kansas, USA; Division of Digestive Diseases, University of Oklahoma Health Sciences Center, Oklahoma City, Oklahoma, USA[b]; and Cardiovascular Biology Research Program, Oklahoma Medical Research Foundation, Oklahoma City, Oklahoma, USA[d]

Notch and Wnt/β-catenin signals play essential roles in intestinal development and homeostasis. *Citrobacter rodentium* induces transmissible murine colonic hyperplasia (TMCH) and various degrees of inflammation, depending upon the genetic background. We aimed at delineating the role of the Notch and Wnt/β-catenin pathways in the regulation of colonic crypt hyperplasia and/or colitis following *C. rodentium* infection. During TMCH, relative levels of the Notch intracellular domain (NICD) increased significantly, along with increases in Jagged-1 and Hes-1 coinciding with the progression and regression phases of hyperplasia. Blocking of Notch signaling with dibenzazepine (DBZ) for 5 days before the onset of hyperplasia also blocked Wnt/β-catenin signaling. Targeting the Notch pathway for 5 days after the onset of hyperplasia failed to inhibit Wnt/β-catenin-regulated crypt hyperplasia. Chronic DBZ administration for 10 days blocked both Notch and Wnt signaling, disrupted the intestinal barrier, and induced colitis. Core-3$^{-/-}$ mice, which are defective in mucin secretion and are susceptible to experimental triggers of colitis, also exhibited significant colitis in response to *C. rodentium* plus DBZ. Chronic DBZ administration in these mice did not result in depletion of the putative stem cell marker doublecortin-like kinase-1 (DCLK1) in the crypts. Dietary bael (*Aegle marmelos*) extract (4%) and curcumin (4%) restored signaling via the Notch and Wnt/β-catenin pathways, thereby promoting crypt regeneration, and also replenished the mucus layer, leading to amelioration of *C. rodentium*- and DBZ-induced colitis in NIH:Swiss mice. Thus, the balancing act between cell proliferation and mucus production to restore barrier integrity seems to depend upon the interplay between the Wnt/β-catenin and Notch pathways in the TMCH model.

The Notch signaling pathway is a key determinant of intestinal epithelial cell self-renewal and of allocation of these cells to specific differentiation lineages (29). In mammals, four Notch genes are expressed, each of which encodes a single-pass transmembrane receptor (Notch1 to [hyphen]4). Each Notch receptor can be activated by cell membrane-associated ligands belonging to the Jagged and Delta-like families. Upon ligand binding, Notch receptors are ultimately cleaved by γ-secretase and other proteases, thereby facilitating nuclear translocation of the Notch intracellular domain (NICD) to regulate transcription of downstream target genes such as the hairy and enhancer of split (Hes) gene and Hey family members (8). Hes-1 is a basic helix-loop-helix (bHLH) transcriptional repressor induced by the Notch signal, while mouse atonal homolog 1 (Math-1) (8) is another bHLH transcription factor and is repressed by Hes-1.

Conditional gut-specific inactivation of the DNA binding protein RBP-Jκ (recombination signal sequence-binding protein Jκ), which mediates signaling by all four Notch receptors, results in a complete loss of proliferating crypt progenitors and their conversion into postmitotic goblet cells. Similarly, rodents treated with the γ-secretase inhibitor dibenzazepine (DBZ) display a huge increase in goblet cell numbers in the gut, thereby mimicking the phenotype of RBP-Jκ mice (33). Conversely, transgenic overexpression of NICD results in a block of secretory cell differentiation, leading to expansion of immature progenitors. Thus, Notch signaling acts as a gatekeeper of the gut progenitor compartment; however, its role in tissue regeneration following intestinal damage is less well understood.

The Wnt signaling pathway plays a crucial role during development of different tissues and organisms. A multiprotein complex including the adenomatosis polyposis coli (APC) protein, axin, and glycogen synthase kinase 3β (GSK-3β) regulates β-catenin protein levels. Activation of canonical Wnt signaling results in GSK-3β inhibition, stabilization and nuclear accumulation of β-catenin, and subsequent activation of lymphoid enhancer factor/T cell factor (LEF1/TCF) target genes (24). Canonical Wnt target genes such as c-*myc*, *cyclinD1*, *MMP7*, *Tcf1*, and *EphB2*, in addition to the Notch target gene *hes1*, have increased expression in the tumors of these mice (31). Thus, accurate coordination of Notch and Wnt signals is indispensable for the maintenance of intestinal homeostasis, since perturbation in these pathways may lead to inflammation or tumorigenesis.

The epithelium and the mucus layer in the intestinal tract form a physical barrier between the potential toxic and noxious agents present in the gut lumen and the underlying tissues. During inflammatory bowel disease (IBD), contact between intestinal bacteria and mucosal surfaces may trigger and perpetuate colonic

Received 7 March 2012 **Returned for modification** 14 April 2012
Accepted 10 June 2012
Published ahead of print 18 June 2012
Editor: S. M. Payne
Address correspondence to Shahid Umar, sumar@kumc.edu.
Supplemental material for this article may be found at http://iai.asm.org/.

doi:10.1128/IAI.00236-12

inflammation (19). Mouse colonic mucus, which is secreted by goblet cells, consists of two layers extending 150 μm above the epithelial cells. The inner layer is densely packed, firmly attached to the epithelium, and devoid of bacteria. In contrast, the outer layer is movable, has an expanded volume due to proteolysis of the Muc-2 mucin, and is colonized by bacteria (11). Alterations in the properties of mucus are well documented for IBD (20), but the pathogenic relevance of these changes remains elusive. We hypothesized that a lack of critical signaling via the Notch and Wnt/β-catenin pathways to regenerate colonic crypts and the altered mucosal barrier contribute to disease pathogenesis following bacterial infection. This hypothesis was tested in an *in vivo* model of hyperproliferation and hyperplasia of the colonic crypts.

Transmissible murine colonic hyperplasia (TMCH), caused by *Citrobacter rodentium*, results in increased proliferation of crypt epithelial cells in the distal colon in adult mice of many outbred stocks, without associated injury or significant histological inflammation (2). In genetically susceptible inbred strains, however, retarded growth, diarrhea, dehydration, coat ruffling, hunched posture, and high mortality have been reported (30). Utilizing the *C. rodentium*-induced TMCH model, we have previously shown significant activation of Wnt/β-catenin (23, 24, 28) and NF-κB (5, 34) signaling in the colonic crypts. We also showed that TMCH is diet sensitive, as dietary pectin (6%) as a source of butyrate significantly abrogated hyperplasia and blocked increases in NF-κB activity (5) and β-catenin levels (26). More recently, we have shown that dietary modulation of NF-κB activity via pectin and curcumin (Cur), the active ingredient of the dietary spice turmeric, increases mucosal regeneration *in vivo* following *C. rodentium* infection-induced colitis by therapeutically targeting cell death and promoting cell survival in genetically susceptible C3H/HeNsd mice (6). In this study, we investigated evidence of Notch signaling during TMCH and whether the Notch and Wnt/β-catenin pathways work in tandem to regulate hyperplasia and/or colitis in response to *C. rodentium* infection. We have also shown previously that *Aegle marmelos* (bael), a medicinal plant from India, has potent anticancer properties (25). Similarly, curcumin has antiviral, antioxidant, and anti-inflammatory properties (22). In the current study, therefore, we tested if dietary intervention through curcumin or bael extract (BE) would affect the two signaling pathways to facilitate crypt regeneration following *C. rodentium*-induced pathogenesis.

MATERIALS AND METHODS

Mice. Male *Helicobacter*-free NIH:Swiss mice were procured from Harlan Laboratories, Inc. Core-3$^{-/-}$ mice lacking β-1,3-*N*-acetylglucosaminyltransferase (C3GnT), an enzyme predicted to be important in the synthesis of core-3-derived O-glycans, were generated by targeted homologous recombination in murine CJ7 embryonic stem cells (129/SvlmJ origin) by use of previously described methods (1). Disruption of the C3GnT gene eliminates core-3-derived O-glycans, the primary components of the intestinal mucus layer that overlies the gastrointestinal epithelium. Core-3$^{-/-}$ mice are highly susceptible to experimental triggers of colitis and colorectal adenocarcinoma (1). As control groups, either littermates or wild-type (WT) mice of identical background were used. Animal studies were approved and conducted in accordance with IACUC guidelines.

TMCH, diets, and treatment with the γ-secretase inhibitor DBZ. TMCH was induced in NIH:Swiss and core-3$^{-/-}$ mice by oral inoculation with a 16-h culture of *C. rodentium* (10^8 CFU) (biotype 4280; ATCC), identified as pink colonies on MacConkey agar, as previously described (5, 6, 23, 24, 26, 28, 34). Biotype 4280 is a unique mouse-specific strain that adheres to mature surface colonocytes within the distal colon to induce histopathological changes known as attaching and effacing lesions (2). Adherent bacteria were assayed using reverse transcription-PCR (RT-PCR) analysis of bacterial intimin in whole-tissue extracts (26). Age- and sex-matched control mice received sterile culture medium only. To block Notch signaling *in vivo*, we used a cell-permeable inhibitor of γ-secretase (DBZ) (33) (EMD Chemicals, Inc.). DBZ was finely suspended in 0.5% (wt/vol) hydroxypropylmethylcellulose (HPMC) and 0.1% (wt/vol) Tween 80 in water and given to mice intraperitoneally (at 10 μmol/kg of body weight) either for 5 consecutive days beginning at 2 days or 7 days postinfection or for 10 consecutive days beginning at 2 days post-*C. rodentium* infection. For dietary intervention, mice were randomized to receive either a control AIN-93 diet synthesized by Harlan Teklad (Madison, WI) or a 4% curcumin and/or 4% bael extract diet. All dietary interventions began at 2 days post-*C. rodentium* infection as described previously (6, 26). Animals were euthanized at 0, 6, or 12 days postinfection, and distal colons were removed to isolate crypts as described previously (5, 6, 23, 24, 26, 28, 34). Briefly, distal colons were attached to a paddle and immersed in Ca^{2+}-free standard Krebs-buffered saline (107 mmol/liter NaCl, 4.5 mmol/liter KCl, 0.2 mmol/liter NaH_2PO_4, 1.8 mmol/liter Na_2HPO_4, 10 mmol/liter glucose, and 10 mmol/liter EDTA), gassed with 5% CO_2 and 95% O_2, at 37°C for 10 to 20 min. Individual crypt units were then separated from the submucosa/musculature by intermittent (30 s) vibration in ice-cold potassium gluconate-HEPES-saline (100 mmol/liter potassium gluconate, 20 mmol/liter NaCl, 1.25 mmol/liter $CaCl_2$, 1 mmol/liter $MgCl_2$, 10 mmol/liter HEPES, 10 mmol/liter glucose, and 5 mmol/liter sodium pyruvate) and 0.1% bovine serum albumin (BSA). The isolated crypts were processed for biochemical and molecular assays.

RNA extraction and semiquantitative and real-time PCRs. Total RNA was extracted from isolated colonic crypts by using Tri reagent. Total cDNA was synthesized by using Superscript II polymerase and random primers. Gene products specific to Hes-1, Math-1, and Muc-2 were identified by performing semiquantitative PCR using a 1/20 dilution of the cDNA. For each gene product, the amplification cycle number was chosen empirically within the linear range. Primer sequences and PCR product sizes are provided in Table S1 in the supplemental material. The PCR products were separated by polyacrylamide gel electrophoresis (PAGE) and visualized by ethidium bromide staining of the gels under UV light. Gel data were recorded with a Bio-Rad FluorS imaging system, and relative densities of the bands were determined with Quantity One software (Bio-Rad, Hercules, CA). Gene expression was normalized with β-actin expression. Total RNA samples were also subjected to real-time PCR with SYBR chemistry (SYBR green I; Molecular Probes, Eugene, OR) for amplification of specific transcripts by use of gene-specific primers and Jumpstart *Taq* DNA polymerase (Sigma-Aldrich, St. Louis, MO). The crossing threshold value assessed by real-time PCR was noted for the transcripts and normalized with that of β-actin mRNA. Changes in mRNA levels are expressed as mean fold changes relative to the control ± standard errors of the means (SEM).

Luciferase reporter gene assay. Transfection experiments were carried out using Lipofectamine 2000 reagent (Invitrogen Life Technologies) according to the manufacturer's instructions. Young adult mouse colonic (YAMC) cells were seeded in 24-well plates at a density of 2×10^5 cells per well and maintained in RPMI 1640 medium supplemented with 10% fetal bovine serum, 2 mM glutamine, 50 μg/ml gentamicin, 100 units/ml penicillin, 100 μg/ml streptomycin, and 5 units/ml gamma interferon (IFN-γ) in a humidified incubator with 5% CO_2 at 33°C. For experiments, cells were incubated at 33°C in IFN-γ-containing medium for 24 h and then transferred to 37°C in IFN-γ-free RPMI 1640 medium for 24 h. For transient-transfection reactions, cells were cotransfected with a Tcf-4 reporter plasmid (TOPFlash) or a plasmid encoding a mutant Tcf binding site (FOPFlash) along with the pRL-TK *Renilla* vector as an internal control. At 24 h posttransfection, cells were infected with *C. rodentium* at a multiplicity of infection (MOI) of 90 or incubated in medium alone (as a control) for 3 h at 37°C in 5% CO_2. After 3 h, the medium was changed

and replaced with fresh medium plus antibiotics to ensure the complete absence of live bacteria. Cells were then treated with either vehicle or DBZ (0.1 μM) for 48 h. Luciferase activity was determined with a luminometer, and the values were normalized to the internal control. All transfection experiments were repeated at least three times.

Western blotting. Total crypt cellular or nuclear extracts (30 to 100 μg protein/lane) were subjected to SDS-PAGE and electrotransferred to a nitrocellulose membrane. The efficiency of electrotransfer was checked by back staining gels with Coomassie blue and/or by reversible staining of the electrotransferred proteins directly on the nitrocellulose membrane with Ponceau S solution. No variability in transfer was noted. Destained membranes were blocked with 5% nonfat dried milk in Tris-buffered saline (TBS) (20 mM Tris-HCl and 137 mM NaCl, pH 7.5) for 1 h at room temperature (21°C). Antigenicity was detected by incubating the membranes overnight with the appropriate primary antibodies (0.5 to 1.0 μg/ml in TBS containing 0.1% Tween 20 [TBS-Tween]; Sigma). After being washed, membranes were incubated with horseradish peroxidase (HRP)-conjugated anti-goat, anti-mouse, or anti-rabbit secondary antibody and developed using the ECL detection system (Amersham Biosciences) according to the manufacturer's instructions.

Histology and histological colitis scores. For histology, tissues were freshly harvested from mice and fixed with 10% neutral buffered formalin or in Carnoy's fixative (60% methanol, 30% chloroform, and 10% acetic acid) prior to paraffin embedding. Paraffin-embedded sections (5 μm) were stained with hematoxylin and eosin (H&E) for gross morphology and with Alcian blue to detect goblet cells. The pictures were obtained with an Eclipse E1000 microscope (Nikon). We determined the histological score according to the following criteria: 0, no signs of inflammation; 1, low level of leukocyte infiltration; 2, moderate level of leukocyte infiltration; 3, high level of leukocyte infiltration, high vascular density, and thickening of bowel wall; and 4, transmural infiltrations, loss of goblet cells, high vascular density, and strong bowel wall thickening.

Immunohistochemistry. Immunohistochemistry to detect CD3, F4/80, Hes-1, claudin-5, and Ki-67 was performed on 5-μm-thick paraffin-embedded sections prepared from distal colons of uninfected normal mice and *C. rodentium*-infected or *C. rodentium*-infected and DBZ-treated mice by utilizing the HRP-labeled polymer conjugated to a secondary antibody, using Envision+System HRP (DAB; DakoCytomation, Carpinteria, CA) with microwave accentuation as described previously (5, 6, 27). Antibody controls included either omission of the primary antibody or detection of endogenous IgG staining with goat anti-mouse or anti-rabbit IgG (Calbiochem, San Diego, CA). Visualization was carried out using either light microscopy (immunohistochemistry) or confocal microscopy.

Electron microscopy. Samples of distal colons from uninfected normal mice or *C. rodentium*-infected or *C. rodentium*-infected and DBZ-treated mice were minced into small cubes, fixed in 4% paraformaldehyde and 2% glutaraldehyde in cacodylate buffer (0.1 M sodium cacodylate, pH 7.6) overnight at room temperature, and postfixed in 1% osmium tetroxide for 90 min. The fixed tissues were dehydrated through a graded series of ethanols, embedded in Epon-araldite resin, and maintained for 48 h at 60°C for polymerization. Ultrathin (100 nm) sections cut on a Leica UC-6 ultramicrotome were placed on glow-discharged 300-mesh copper grids and stained with uranyl acetate and Sato's lead to enhance contrast. Ultrathin sections were examined with a Hitachi H-7600 electron microscope.

FITC-D assay. An *in vivo* permeability assay to assess epithelial barrier function was performed using fluorescein isothiocyanate-dextran (FITC-D) as described previously (16). Briefly, food was withdrawn for 4 h from 5- to 6-week-old mice in various groups, and animals were subjected to gavage with 80 mg FITC-D/100 g body weight (molecular weight of FITC-D, 4,000; Sigma-Aldrich). Serum was collected at the time of euthanasia, blood cells were removed by centrifugation, and the fluorescence intensity of each sample was measured with a fluorimeter (excitation wavelength, 492 nm; emission wavelength, 525 nm) (FLUOstar Galaxy 2300; BMG Labtech, Durham, NC). FITC-D concentrations were determined from standard curves generated by serial dilution of FITC-D, and permeability was calculated by linear regression of sample fluorescence (Excel 5.0; Microsoft).

Statistical analysis. All experimental results are expressed as mean values ± standard errors. Statistical analyses of all studies were performed using unpaired, two-tailed Student's *t* tests and one-way analysis of variance (ANOVA) for multiple-group comparisons (Prism 5; GraphPad, San Diego, CA). *P* values of <0.05 were considered significant.

RESULTS

Evidence of Notch signaling in TMCH. Utilizing the TMCH model, we recently characterized days 6 and 12 post-*C. rodentium* infection as "progression" of hyperplasia and days 20 through 34 postinfection as "regression" of hyperplasia (5). In the current study, during analyses of the Notch pathway, relative levels of NICD in colonic crypt extracts were increased significantly at day 6 compared to those for uninfected controls and peaked by day 12 (Fig. 1A, panel i), thereby correlating with peak hyperplasia (24). At days 20, 27, and 34, a declining trend consistent with regression of hyperplasia was observed (Fig. 1A, panels i and ii). We next determined the relative mRNA expression of both Hes-1 and Math-1 in the distal colonic crypts of uninfected or *C. rodentium*-infected mice. Total RNA samples subjected to real-time RT-PCR exhibited significant upregulation of Hes-1 mRNA at day 6, which peaked by day 12 before going through a declining phase at days 20, 27, and 34 (Fig. 1B). Math-1 mRNA levels, on the other hand, exhibited significant expression in uninfected controls, with sequential decreases at days 6 and 12 of TMCH (Fig. 1B). Interestingly, Math-1 expression gradually increased at days 20, 27, and 34, in contrast to Hes-1 expression, and coincided with regression of hyperplasia (5, 24). We next analyzed components of the Notch pathway at the protein level. In the crypt cellular extracts, relative levels of Jagged-1 were undetectable for uninfected controls (Fig. 1Ci). A sequential increase starting at day 6, followed by an ~6-fold increase at day 12, accompanied *C. rodentium*-induced peak hyperplasia (Fig. 1Ci). At day 20, however, a 50% decrease in the cellular abundance of this protein followed the declining trend at days 27 and 34 of TMCH (Fig. 1Ci). In nuclear extracts, Hes-1 levels were increased significantly at day 6 and profoundly at day 12 compared to those in uninfected controls and remained elevated to significant levels at days 20 and 27 before declining by day 34 (Fig. 1Ci). Math-1 levels in the crypt nuclear extracts increased significantly in uninfected control mice compared to the levels recorded at days 6 and 12 (Fig. 1Ci). At days 20, 27, and 34, however, a gradual increase in Math-1 protein levels was recorded (Fig. 1Ci and ii). During immunostaining for Hes-1, a few scattered cells along the length of the colonic crypt exhibited nuclear staining in uninfected controls (Fig. 1D). At day 6, and particularly at day 12, intense nuclear immunoreactivity extending throughout the longitudinal crypt axis was recorded (Fig. 1D). At days 20, 27, and 34, a downward trend of Hes-1 immunoreactivity was observed (Fig. 1D). Thus, activation of the Notch pathway during TMCH may be integral to the regulation of crypt hyperproliferation/hyperplasia in response to *C. rodentium* infection.

Consequence of blocking Notch signaling *in vivo*. We next designed experiments to block Notch signaling *in vivo* through the γ-secretase inhibitor DBZ. The approach to blocking Notch signaling was 2-fold: (i) to target the Notch pathway before and after the onset of hyperplasia and (ii) to block Notch signaling chronically to see if hyperplasia was abrogated. Acute (5 days) treatment

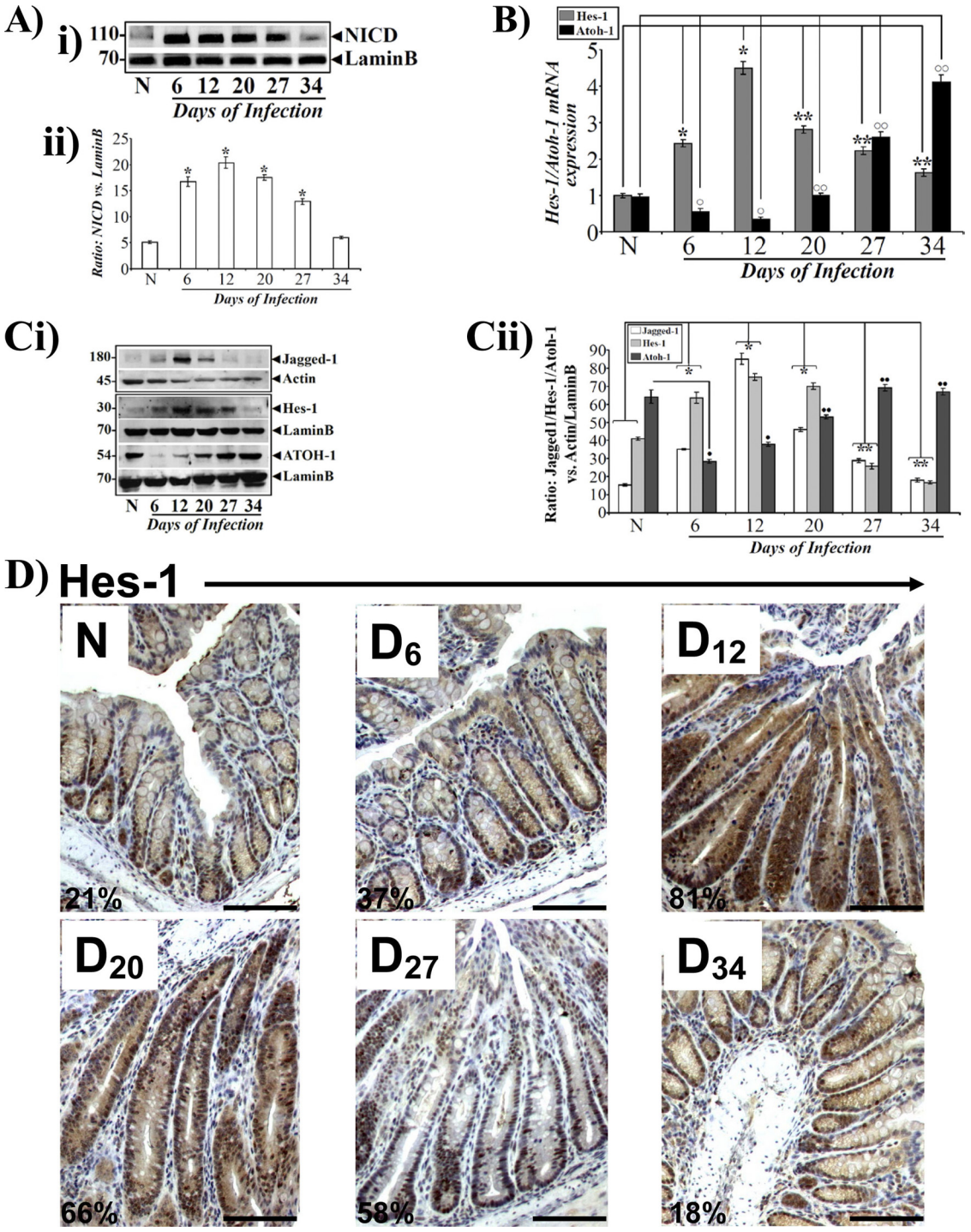

FIG 1 Evidence of Notch signaling in the TMCH model. (A) Relative levels of NICD in colonic crypt cellular extracts prepared from uninfected normal (N) NIH:Swiss mice and infected NIH:Swiss mice at days 6 to 34 postinfection are shown as Western blots (i) and a bar graph (ii). *, $P < 0.05$ versus controls; $n = 3$ independent experiments. (B) Real-time RT-PCR. Total RNAs were isolated from the crypts of the animals described for panel A and subjected to real-time RT-PCR for the indicated genes. *, $P < 0.05$ versus controls; **, $P < 0.05$ versus day 12; ○, $P < 0.05$ versus controls; ○○, $P < 0.05$ versus day 12; $n = 3$ independent experiments. (C) Relative levels of Jagged-1, Hes-1, and Math-1 in the colonic crypts of uninfected normal (N) NIH:Swiss mice and infected NIH:Swiss mice at days 6 to 34 postinfection are shown as Western blots (i) and a bar graph (ii). *, $P < 0.05$ versus controls; **, $P < 0.05$ versus day 12; ●, $P < 0.05$ versus controls; ●●, $P < 0.05$ versus day 12; $n = 3$ independent experiments. (D) Paraffin-embedded sections showing percentages of cells stained for Hes-1. Bars = 100 μm; $n = 3$ independent experiments.

with DBZ beginning on the 2nd day of *C. rodentium* infection (i.e., before the onset of hyperplasia) (24) caused a significant increase in goblet cells compared to the level with vehicle alone (Fig. 2B), without any gross change in morphology (Fig. 2A), and inhibited crypt hyperplasia (Fig. 2C). These changes were associated with decreases in NICD (Fig. 2D, panels i and ii) and in mRNA and protein levels of Hes-1 (Fig. 2E, panels i and ii, and F, panels i and ii), β-catenin (Fig. 2F, panels i and ii), and Jagged-1 (Fig. 2F, panels i and ii) and with upregulation of Math-1 (Fig. 2E, panels i and ii, and F, panels i and ii). Acute DBZ treatment beginning on the 7th day of *C. rodentium* infection (i.e., after the onset of hyperplasia) (5, 24) followed by euthanasia at day 12 also increased goblet cells and inhibited NICD compared to the levels with vehicle alone, leading to inhibition of Notch signaling in colonic crypts (Fig. 2D to F). Interestingly, late blocking of Notch signaling did not inhibit β-catenin, Jagged-1, or crypt hyperplasia.

In the second approach, where animals were given DBZ for 10 consecutive days beginning on the 2nd day of *C. rodentium* infection followed by euthanasia at day 12, we observed a blockade of both Notch and Wnt signaling. *C. rodentium* infection alone led to significant crypt hyperplasia (Fig. 3A), with an almost complete loss of goblet cells (Fig. 3B), as reported earlier (2). In response to chronic DBZ administration, goblet cells increased dramatically (Fig. 3B), with a concomitant blockade of NICD generation (Fig. 3C, panel i) leading to inhibition of Hes-1 at the mRNA (Fig. 3C, panel ii) and protein (Fig. 3D, panel i) levels. On the other hand, Math-1 mRNA and protein levels increased significantly in crypts from DBZ-treated mice (Fig. 3C, panel ii, and D, panel i). We next investigated the effects of chronic Notch inhibition on components of the Wnt pathway. Chronic DBZ treatment also blocked increases in both β-catenin phosphorylated at Ser-552 (active β-catenin) (24) and total β-catenin (Fig. 3D, panel ii), leading to downregulation of the downstream targets Jagged-1 (Fig. 3D, panel i) and cyclin D1 (Fig. 3D, panel ii), respectively, coinciding with abrogation of hyperplasia (Fig. 3F). To directly establish a link between the Notch and Wnt pathways, we next studied the transcription of β-catenin/Tcf target genes in YAMC cells in response to *C. rodentium* infection and following DBZ treatment. YAMC cells were transfected with luciferase reporter plasmids encoding either wild-type (TOPFlash) or mutant (FOPFlash) Tcf binding sites along with a *Renilla* luciferase plasmid. Subsequent *C. rodentium* infection increased β-catenin-dependent TOPFlash reporter activity, while DBZ treatment led to an ~55% reduction in reporter activity, suggesting a link between the two pathways (Fig. 3E). At the same time, neither *C. rodentium* nor *C. rodentium* plus DBZ had any effect on FOPFlash reporter activity (Fig. 3E). Interestingly, in response to chronic Notch inhibition, we also observed significant colitis in otherwise colitis-resistant NIH:Swiss mice: *C. rodentium*-infected mice receiving DBZ for 10 days, in contrast to those receiving *C. rodentium* alone, had dilated and thickened walls with significant ulceration and bleeding, as well as increases in colon weight (Fig. 4A and B). Transmission electron microscopy revealed a significant bacterial presence at the luminal surface in untreated *C. rodentium*-infected mice compared to *C. rodentium*-infected mice receiving DBZ (Fig. 4C). In sections from *C. rodentium*-infected and DBZ-treated mice, however, while fewer bacteria were seen at the surface, they could be seen reaching the epithelium and were detected deep down and along the sides of the crypts (Fig. 4C). This is consistent with studies of Muc-2$^{-/-}$ mice, which exhibit significant bacterial translocation, slow growth, and spontaneous colitis by 7 weeks of age (11). In the current study, further evaluation of the colons of *C. rodentium*-infected and DBZ-treated mice showed high levels of leukocyte and polymorphonuclear leukocyte (PMN) infiltration. Figure 4Di shows representative images of H&E-stained sections, while Fig. 4Dii illustrates the average histological scores. During staining with Alcian blue, which recognizes acidic carbohydrates, DBZ-treated mice had a disrupted mucinous gel layer compared to untreated *C. rodentium*-infected mice (Fig. 4Ei, arrows), and they also exhibited a significant increase in serum FITC-dextran compared to untreated *C. rodentium*-infected mice (Fig. 4Eii), indicating increases in paracellular permeability. To link these changes to disruption of tight junctions, several proteins involved in tight junction formation and maintenance were investigated. We observed significant decreases in transmembrane claudins 2 and 5, along with a loss of the peripheral ZO-1 and ZO-2 proteins, in crypts from *C. rodentium*-infected and DBZ-treated mice compared to those from untreated *C. rodentium*-infected mice (Fig. 4F). Immunohistochemistry also revealed a significant reduction in claudin-5 staining in sections from *C. rodentium*-infected and DBZ-treated mice compared to those from untreated *C. rodentium*-infected mice (Fig. 4G). We next homogenized livers and spleens along with distal colons from the above group of animals and plated the homogenates on selective MacConkey agar plates. Bacterial counts in the colons from untreated *C. rodentium*-infected mice were significantly higher than those for *C. rodentium*-infected mice receiving DBZ, despite a lack of any inflammatory axis in untreated *C. rodentium*-infected mice (Table 1). At the same time, significantly more viable bacteria were recovered from the livers and spleens of DBZ-treated mice than from those of untreated *C. rodentium*-infected mice (Table 1), suggesting that alterations in tight junctions may have facilitated bacterial dissemination into distant organs. Since Notch signaling has been implicated in the maintenance of intestinal stem cells, we next explored the effects of blocking Notch signaling *in vivo* on expression of the putative stem cell marker doublecortin-like kinase 1 (DCLK1) in the distal colons of mice in various groups. Interestingly, despite acute or chronic blockade of the Notch pathway, DCLK1 expression in *C. rodentium*-infected mice receiving DBZ was not any different from that in either uninfected or *C. rodentium*-infected mice without treatment (Fig. 4H). Thus, chronic inhibition of the Wnt/Notch pathway cripples the ability of the colonic mucosa to regenerate itself, but not necessarily due to a loss of colonic stem cells. In summary, these data suggest that disruption of tight junctions may have contributed to disease pathogenesis following *C. rodentium* and DBZ administration.

When paraffin-embedded sections were stained for CD3$^+$ T cells and F4/80$^+$ macrophages, we observed slight increases in these cells in distal colons from *C. rodentium*-infected mice; for *C. rodentium*-infected mice receiving DBZ, a profound expansion of both T cells and macrophages was recorded, predominantly in the submucosal regions, in addition to recruitment along the length of the colonic crypts (data not shown). To rule out the possibility that DBZ may be toxic on its own, uninfected NIH:Swiss mice were given daily intraperitoneal injections of DBZ at 10 μmol/kg for 10 days and their mucosae examined for possible effects. DBZ caused goblet cell hyperplasia, as expected, without altering (i) epithelial permeability, (ii) cell proliferation, or (iii) message or protein levels of Hes-1 and Math-1 (see Fig. S1A to S1F in the

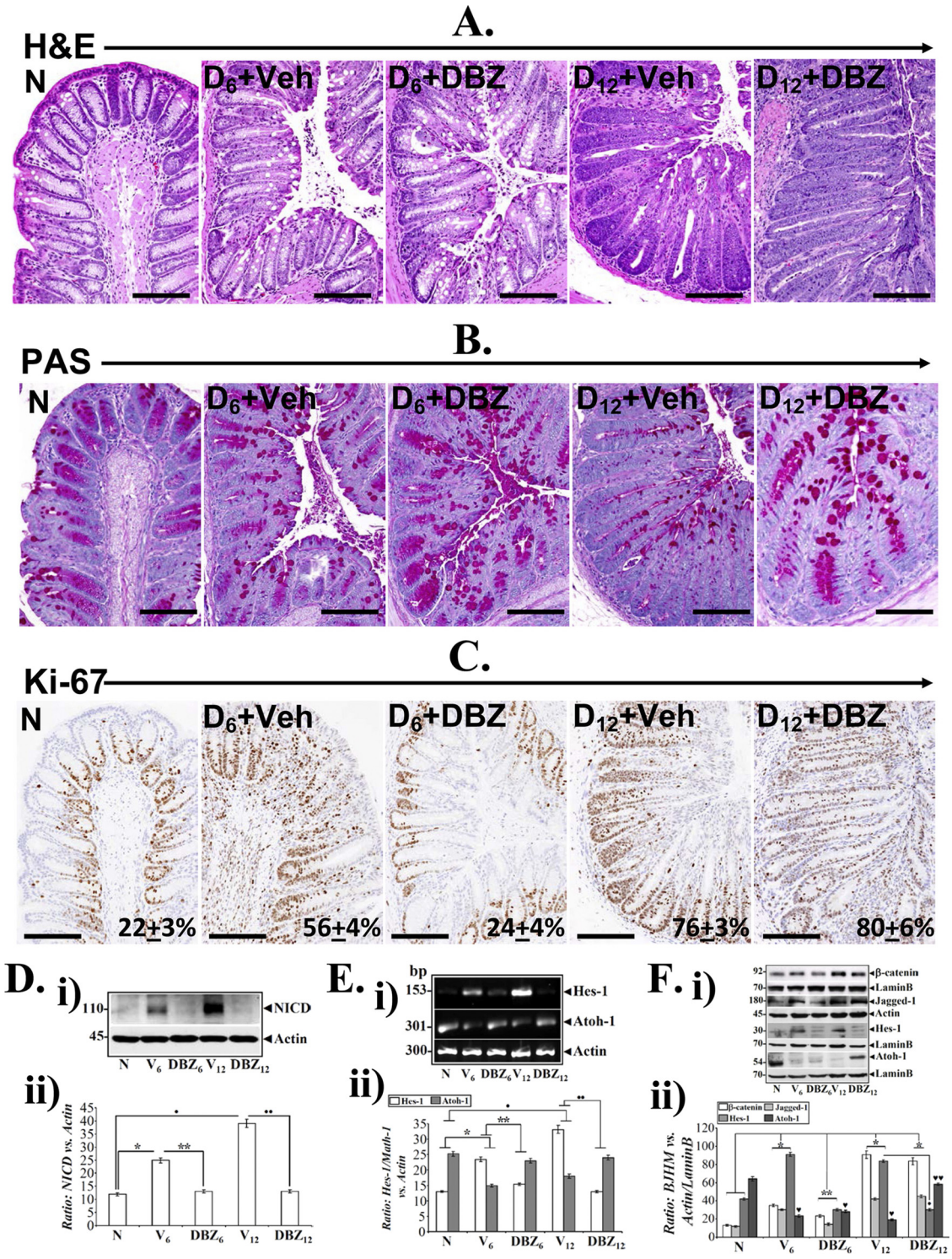

FIG 2 Strategies to block Notch signaling *in vivo*. Uninfected normal (N) NIH:Swiss mice were infected with *C. rodentium* and either received vehicle (Veh) or DBZ for 5 days followed by euthanasia at day 6 (D_6+Veh and D_6+DBZ) or received Veh or DBZ for 5 days followed by euthanasia at day 12 (D_{12}+Veh and D_{12}+DBZ). Paraffin-embedded sections were analyzed by H&E (A), periodic acid-Schiff (PAS) (B), and Ki-67 (C) staining. Numbers in panel C represent percentages of cells stained for Ki-67. Bars = 100 μm; $n = 3$ independent experiments. (D) Colonic crypt cellular extracts prepared from uninfected normal mice (N), *C. rodentium*-infected and vehicle-treated mice at day 6 or 12 (V_6 or V_{12}), or *C. rodentium*-infected and DBZ-treated mice (DBZ_6 or DBZ_{12}) are shown as Western blots (i) and a bar graph (ii). *, $P < 0.05$ versus controls; **, $P < 0.05$ versus V_6; ●, $P < 0.05$ versus controls; ●●, $P < 0.05$ versus V_{12}; $n = 3$ independent experiments. (E) RT-PCR (i) and bar graph (ii) analyses of total crypt RNA for the indicated gene products. *, $P < 0.05$ versus controls; **, $P < 0.05$ versus V_6; ●, $P < 0.05$ versus controls; ●●, $P < 0.05$ versus V_{12}; $n = 3$ independent experiments. (F) Western blots (i) and bar graph (ii) showing crypt cellular/nuclear levels of β-catenin, Jagged-1, Hes-1, and Math-1. *, $P < 0.05$ versus controls; **, $P < 0.05$ versus V_6; ●, $P < 0.05$ versus V_{12}; ♥, $P < 0.05$ versus controls; ♥♥, $P < 0.05$ versus V_{12}; $n = 3$ independent experiments.

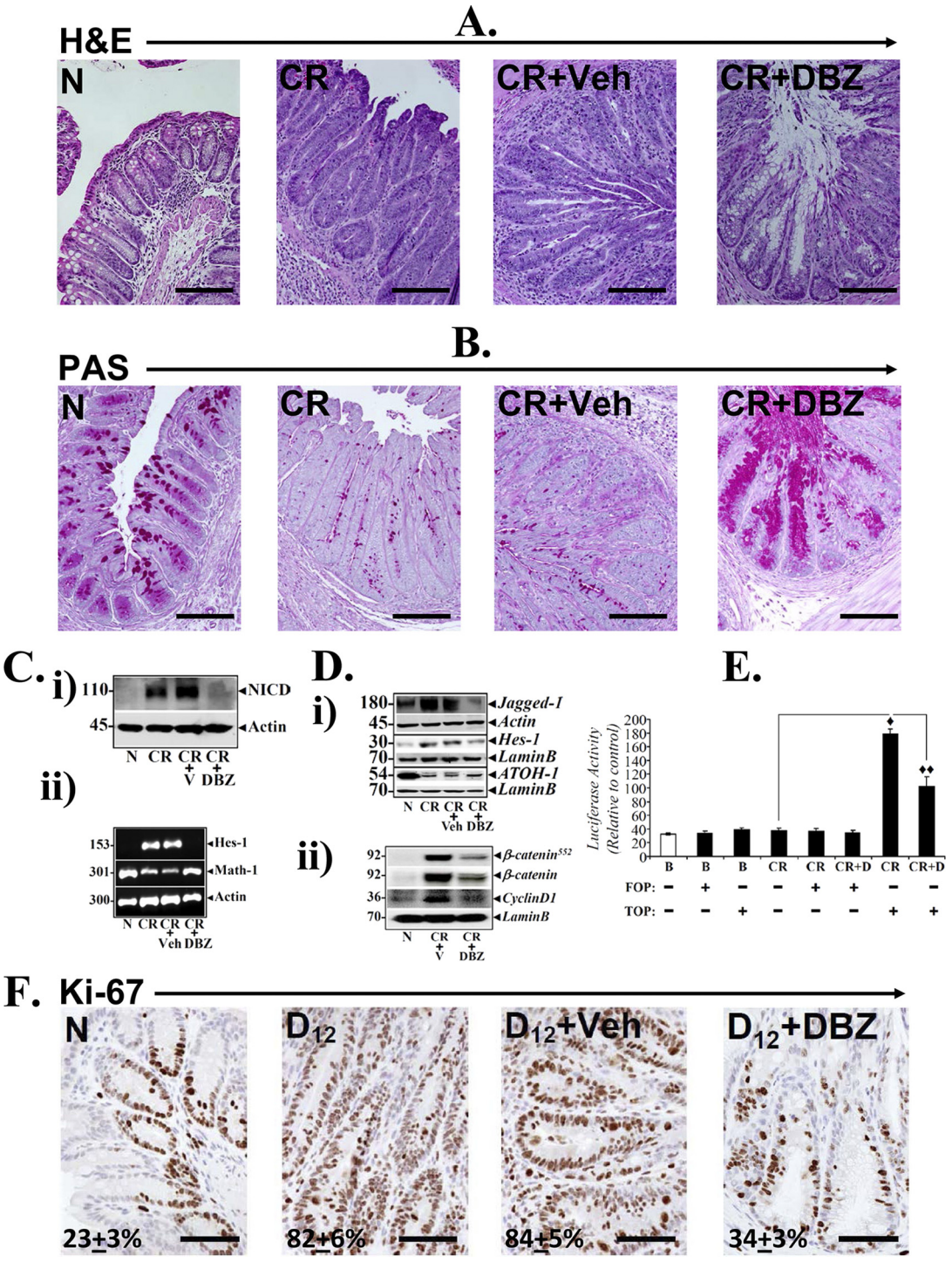

FIG 3 Chronic DBZ treatment blocks both Notch and Wnt signaling and abrogates hyperplasia. Uninfected normal (N) NIH:Swiss mice were infected with *C. rodentium* alone for 12 days (CR) or received either vehicle (CR+Veh) or DBZ (CR+DBZ) for 10 days, and their colons were analyzed by H&E (A) and PAS (B) staining. (C) Western blots (i) and RT-PCR results (ii) showing relative levels of NICD, Hes-1, and Math-1 in the colonic crypts of uninfected normal mice (N), *C. rodentium*-infected mice (CR), *C. rodentium*-infected and vehicle-treated mice (CR+V), or *C. rodentium*-infected and DBZ-treated (CR+DBZ) mice. $n = 3$ independent experiments. (D) (i) Western blots showing crypt nuclear levels of Jagged-1, Hes-1, and Math-1. (ii) Western blots showing crypt nuclear levels of β-catenin phosphorylated at Ser-552 in relation to total β-catenin and cyclin D1. (E) *C. rodentium* infection induces β-catenin/Tcf-dependent transcriptional activity *in vitro*. YAMC cells were cotransfected with a Tcf-4 reporter plasmid (TOPFlash; TOP) or a plasmid encoding a mutant Tcf binding site (FOPFlash; FOP) and the pRL-TK *Renilla* vector as an internal control. At 24 h posttransfection, cells were infected with *C. rodentium* at an MOI of 90 or with medium alone (as a control) for 3 h at 37°C in 5% CO_2. Cells were then treated with either vehicle or DBZ (0.1 μM) for 48 h. Luciferase activity was determined with a luminometer, and the values were normalized to the internal control level. ◆, $P < 0.05$ versus *C. rodentium*-infected controls; ◆◆, $P < 0.05$ versus CR+TOPFlash plasmid; $n = 3$ independent experiments. (F) Paraffin-embedded sections showing percentages of cells stained for Ki-67. Bars = 50 μm; $n = 3$ independent experiments.

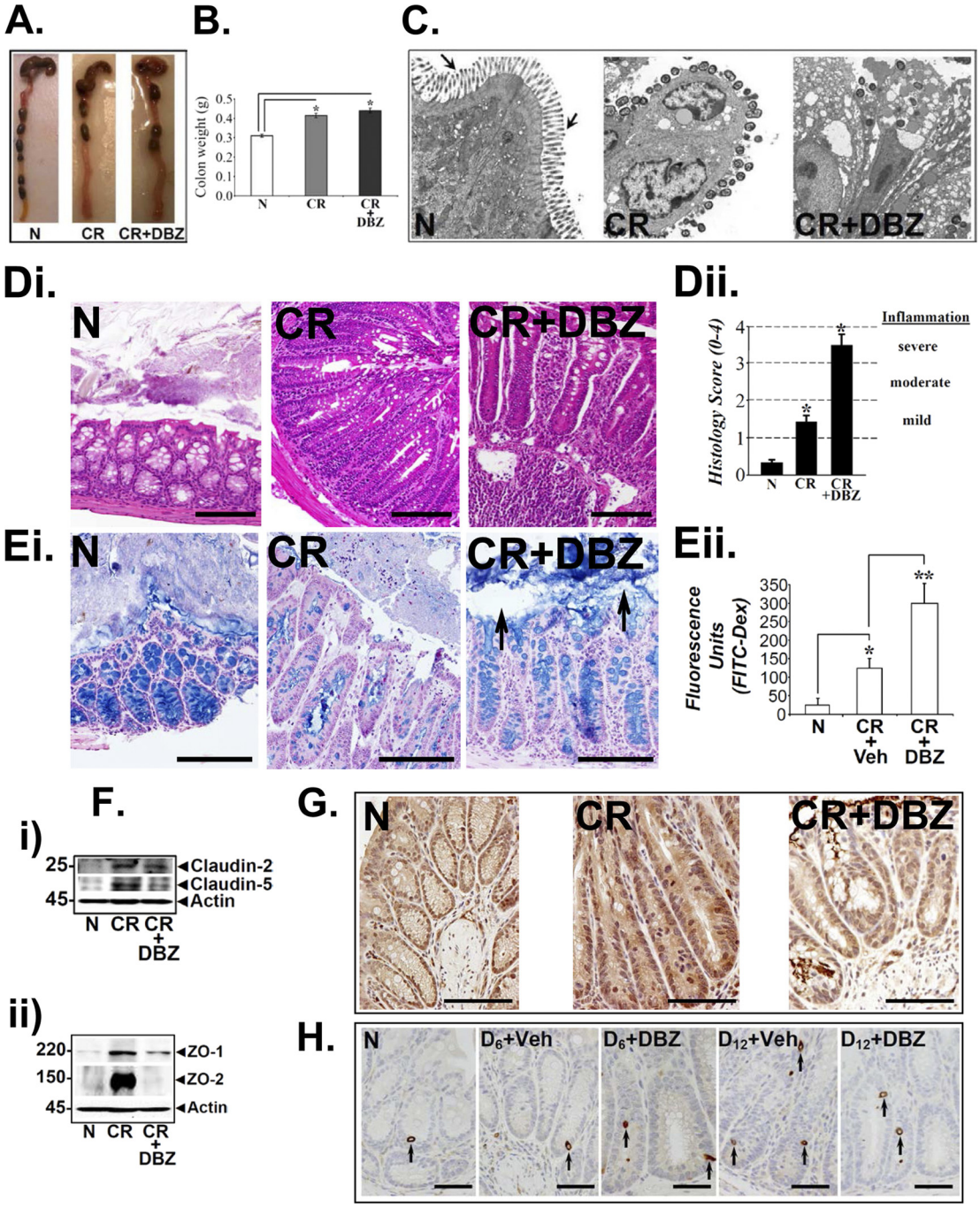

FIG 4 Chronic DBZ treatment increases paracellular permeability and bacterial dissemination leading to colitis in NIH:Swiss mice. (A) Representative images of colons from uninfected normal mice (N), *C. rodentium*-infected and vehicle-treated mice (CR), and *C. rodentium*-infected and DBZ-treated (CR+DBZ) mice ($n = 3$ independent experiments). (B) Colonic wet weights for the experimental groups. *, $P < 0.05$ versus controls; $n = 5$ independent experiments. (C) Distal colonic fragments from the above group of mice were subjected to transmission electron microscopy to detect microvilli (black arrows) and the presence of bacteria. Significant bacterial attachment and destruction of microvilli in *C. rodentium*-infected mucosa were exacerbated with DBZ (2.0-μm section; note the bacterial presence deep down and along the sides of the crypt). (D) Paraffin-embedded sections from colons of various groups were fixed in Carnoy's fixative, stained with H&E (i), and analyzed by a certified pathologist to determine the inflammatory score (ii). *, $P < 0.05$ versus controls. (E) (i) Alcian blue-stained sections (arrows point toward the disorganized inner mucinous gel layer in sections from *C. rodentium*-infected and DBZ-treated mice). Bars = 150 μm; $n = 3$ independent experiments. (ii) Uninfected normal (N) NIH:Swiss mice, *C. rodentium*-infected and vehicle-treated mice (CR+Veh), or *C. rodentium*-infected and DBZ-treated mice (CR+DBZ) were subjected to gavage with FITC-D, and serum concentrations, shown as fluorescence units, were measured 4 h later. *, $P < 0.05$ versus controls; **, $P < 0.05$ versus *C. rodentium*-infected and vehicle-treated mice; $n = 3$ independent experiments. (F) Western blots showing tight junction proteins claudin-2 and [hyphen]5 (i) and ZO-1 and [hyphen]2 (ii) for the group of mice described for panel A. (G) Paraffin-embedded sections were stained for claudin-5. Note the significant loss of claudin-5 staining in sections from *C. rodentium*-infected and DBZ-treated mice. Bars = 100 μm; $n = 3$ independent experiments. (H) Paraffin-embedded sections prepared from the distal colons of NIH:Swiss mice after the indicated treatments were stained with antibody for the putative stem cell marker DCLK1 (arrows). Bars = 75 μm; $n = 3$ independent experiments.

TABLE 1 Effects of *C. rodentium* infection and DBZ treatment on bacterial dissemination in NIH:Swiss mice

Tissue	CFU/g of tissue		
	Uninfected mice	*C. rodentium*-infected and vehicle-treated mice	*C. rodentium*-infected and DBZ-treated mice
Colon	0.0	$2{,}826 \times 10^{3a}$	31×10^{3b}
Liver	0.0	$114 \times 10^{3a,c}$	$420 \times 10^{3b,d}$
Spleen	0.0	$83 \times 10^{3a,c}$	$270 \times 10^{3b,d}$

[a] Significant difference in *C. rodentium* counts versus uninfected control levels ($n = 5$ mice/group; $P < 0.05$).
[b] Significant difference in *C. rodentium* counts in *C. rodentium*-infected and DBZ-treated animals versus *C. rodentium*-infected and vehicle-treated animals ($n = 5$ animals/group; $P < 0.05$).
[c] Significant difference in *C. rodentium* counts in liver or spleen versus colon ($n = 5$ animals/group; $P < 0.05$).
[d] Significant difference in *C. rodentium* counts in liver or spleen versus colon ($n = 5$ animals/group; $P < 0.05$).

supplemental material), suggesting that DBZ in the absence of a bacterial infection is not toxic to these mice.

Next, we hypothesized that if colitis in *C. rodentium*-infected and DBZ-treated animals is indeed due to disruption of the mucinous gel layer, then mice defective in colonic mucin may either be equally susceptible or exhibit an exacerbation of colitis and paracellular permeability. To test this hypothesis, we utilized mice lacking core-3 β-1,3-*N*-acetylglucosaminyltransferase, an enzyme important in the synthesis of core-3-derived O-glycans, the primary component of the intestinal mucins. Core-$3^{-/-}$ mice have defects in mucin synthesis and are susceptible to the experimental triggers of colitis but (i) do not exhibit altered barrier function or any increase in recruitment of immune cells to the mucosa in the absence of colitic insult and (ii) do not develop spontaneous colitis (1). Following *C. rodentium* infection of core-$3^{-/-}$ mice, we observed a disrupted intestinal barrier and some evidence of colitis which was severely exacerbated following DBZ administration, as revealed by H&E (Fig. 5A, upper panels) and Alcian blue (Fig. 5A, lower panels) staining, respectively. Figure 5B, panel i, illustrates the average histological scores. Core-$3^{-/-}$ mice infected with *C. rodentium* alone exhibited a 4-fold increase in serum FITC-dextran levels compared to those in uninfected control mice (Fig. 5B, panel ii), while DBZ administration to the infected mice destroyed the barrier function, causing a 21-fold increase in serum FITC-dextran levels (Fig. 5B, panel ii). Similar to the case in NIH:Swiss mice, increases in paracellular permeability in core-$3^{-/-}$ mice were probably due to loss of the tight junction proteins claudin-5 and ZO-1 in the crypts of *C. rodentium*-infected and DBZ-treated mice compared to untreated *C. rodentium*-infected mice (Fig. 5C, panels i and ii). At the molecular level, chronic DBZ administration blocked increases in NICD and Hes-1, upregulated Math-1 (Fig. 5D and E), and also blocked increases in β-catenin and Jagged-1 levels (Fig. 5E), which may have led to abrogation of crypt hyperplasia (Fig. 5F). Mice infected with *C. rodentium* but not treated with DBZ had significantly higher bacterial counts in the colon (Table 2), while DBZ administration to *C. rodentium*-infected mice caused significant bacterial dissemination to the liver and the spleen (Table 2). To rule out the possibility that core-$3^{-/-}$ mice, which are on a C57BL/6 background, are more sensitive to DBZ-induced toxicity than NIH:Swiss mice, uninfected C57BL/6 mice were given daily intraperitoneal injections of DBZ at 10 μmol/kg for 10 days, and their mucosae were examined for possible effects. DBZ caused goblet cell hyperplasia without altering epithelial permeability, cell proliferation, or the components of the Notch and Wnt pathways (data not shown). In addition, similar to the case for NIH:Swiss mice, the changes accrued were not due to reallocation of stem cells into goblet cells, as DCLK1 staining in *C. rodentium*-infected and DBZ-treated mice was similar to that in *C. rodentium*-infected mice without DBZ treatment (Fig. 5G). Thus, both altered barrier function and a lack of active signaling via the Notch/Wnt pathways seem to regulate *C. rodentium*-induced pathogenesis in core-$3^{-/-}$ mice as well.

Efforts to restore signaling via Notch and Wnt/β-catenin pathways through dietary intervention to ameliorate colitis. We hypothesized that dietary intervention may restore the interplay between the Notch and Wnt/β-catenin pathways, thereby helping the mucosa to recover from colitic insult. DBZ administration to *C. rodentium*-infected NIH:Swiss mice for 10 days induced microabscesses, barrier disruption, significant crypt shortening, and colitis (Fig. 6A and B). Diets containing 4% bael extract (BE) and 4% curcumin (Cur) restored the inner mucous gel layer as revealed by Alcian blue staining (Fig. 6B) and, paradoxically, promoted crypt hyperplasia in *C. rodentium*-infected mice receiving DBZ to the levels recorded for mice receiving *C. rodentium* alone (Fig. 6C). This could be due to restoration of Notch signaling, as relative increases in NICD levels (Fig. 6D) led to concomitant upregulation of the Jagged-1 and Hes-1 proteins, but not Math-1 (Fig. 6E and F), in crypts from diet-treated mice. Changes in β-catenin, however, were subtle (Fig. 6F).

Next, we examined the effect of dietary intervention on amelioration of colitis in response to *C. rodentium* plus DBZ by analyzing the components of the mucosal and epithelial barriers. We first focused on Muc-2, the primary component of the gel-forming intestinal mucins (11). The rationale for Muc-2 analysis was 2-fold: (i) Muc-2 is the predominant secretory mucin in the colon, and (ii) mucin polymers must be intact to maintain its protective function. In response to *C. rodentium* infection, we discovered significantly less staining for Muc-2 in the crypts and the lumen than that in uninfected controls (Fig. 7A). *C. rodentium*-infected mice receiving DBZ exhibited an interesting pattern for Muc-2 staining: while Muc-2 staining in the crypt was intense, as one would expect given the goblet cell metaplasia, neither the inner nor the outer mucus layer was significantly stained (Fig. 7A). In response to BE and Cur intervention, we observed dramatic restoration of the inner (Fig. 7A, arrows) and outer (Fig. 7A) mucus layers. The effect of dietary intervention on Muc-2 expression in the crypts was further validated by RT-PCR and Western blotting. Both analyses mirrored the results of Muc-2 staining in the crypts (Fig. 7Bi and ii). When components of the tight junction were examined, we observed significant decreases in both claudins 2 and 5 as well as ZO-2 in crypts from *C. rodentium*-infected and DBZ-treated mice compared to those from mice infected with *C. rodentium* but not treated with DBZ (Fig. 7C and D). In response to dietary intervention, BE restored expression of both claudins 2 and 5, while the curcumin diet was more effective in restoring ZO-2 expression (Fig. 7C and D). It has been shown previously that decreased expression of the solute carrier family 26 member 3 (SLC26A3) protein, also known as downregulated in adenoma (DRA), leads to infectious diarrhea in mice in response to *C. rodentium* infection (4). SLC26A3 has also been implicated in the maintenance of alkaline mucus layers, and loss of this protein may

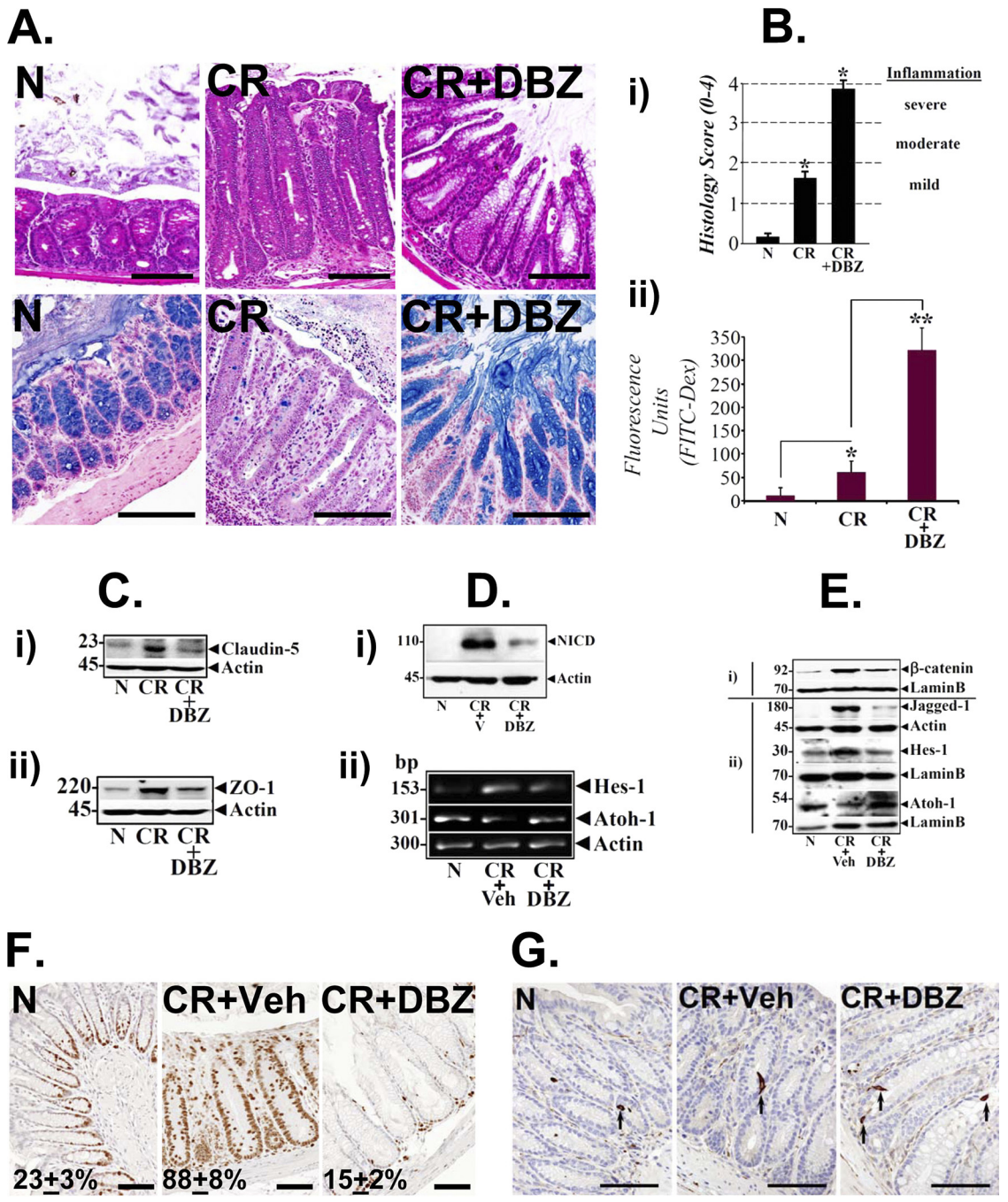

FIG 5 Effect of *C. rodentium* infection and DBZ administration on mice deficient in core-3-derived O-glycans (core-3$^{-/-}$ mice). (A) Paraffin-embedded sections from uninfected normal (N), *C. rodentium*-infected and vehicle-treated (CR), and *C. rodentium*-infected and DBZ-treated (CR+DBZ) core-3$^{-/-}$ mice were analyzed by H&E (upper panels) and Alcian blue (lower panels) staining to detect goblet cells and the inner mucus layer, respectively. Bars = 150 μm; n = 3 independent experiments. (B) (i) Paraffin-embedded sections from the group of mice described for panel A were fixed in Carnoy's fixative and analyzed by a certified pathologist to determine the inflammatory score. *, $P < 0.05$ versus controls; n = 3 independent experiments. (ii) The group of mice described for panel A were subjected to gavage with FITC-D, and serum concentrations, shown as fluorescence units, were measured 4 h later. *, $P < 0.05$ versus controls; **, $P < 0.05$ versus *C. rodentium*-infected mice; n = 3 independent experiments. (C) Western blots showing relative levels of claudin-5 (i) and ZO-1 (ii) in the crypts of group A mice. (D) (i) Relative levels of NICD in the colonic crypts of uninfected normal mice (N), *C. rodentium*-infected and vehicle-treated mice (CR+V), and *C. rodentium*-infected and DBZ-treated mice (CR+DBZ) are shown in Western blots. (ii) RT-PCR analysis of total colonic crypt RNA for the indicated gene products. (E) Western blots showing crypt cellular/nuclear levels of β-catenin (i) and Jagged-1, Hes-1, and Math-1 (ii). n = 3 independent experiments. (F) Paraffin-embedded sections showing percentages of cells positive for Ki-67 staining. Bars = 75 μm; n = 3 independent experiments. (G) Paraffin-embedded sections prepared from the distal colons of NIH:Swiss mice after the indicated treatments were stained with antibody for the putative stem cell marker DCLK1 (arrows). Bars = 75 μm; n = 3 independent experiments.

TABLE 2 Effects of *C. rodentium* infection and DBZ treatment on bacterial dissemination in core-3$^{-/-}$ mice

Tissue	CFU/g of tissue		
	Uninfected mice	*C. rodentium*-infected and vehicle-treated mice	*C. rodentium*-infected and DBZ-treated mice
Colon	0.0	547×10^{3a}	3.8×10^{3b}
Liver	0.0	$34 \times 10^{3a,c}$	$195 \times 10^{3b,d}$
Spleen	0.0	$38 \times 10^{3a,c}$	$122 \times 10^{3b,d}$

[a] Significant difference in *C. rodentium* counts versus uninfected control levels ($n = 5$ mice/group; $P < 0.05$).
[b] Significant difference in *C. rodentium* counts in *C. rodentium*-infected and DBZ-treated animals versus *C. rodentium*-infected and vehicle-treated animals ($n = 5$ animals/group; $P < 0.05$).
[c] Significant difference in *C. rodentium* counts in liver or spleen versus colon ($n = 5$ animals/group; $P < 0.05$).
[d] Significant difference in *C. rodentium* counts in liver or spleen versus colon ($n = 5$ animals/group; $P < 0.05$).

lead to barrier impairment and mucosal inflammation in mice (4, 36). In response to *C. rodentium* infection, we observed upregulation of SLC26A3 compared to that in uninfected controls (Fig. 7E). Following DBZ treatment of *C. rodentium*-infected NIH:Swiss mice, SLC26A3 levels decreased dramatically, coinciding with colitis (Fig. 7E). Both the BE and Cur diets restored SLC26A3 expression in crypts from *C. rodentium*-infected and DBZ-treated mice (Fig. 7E), which coincided with restoration of both the inner mucus layer and tight junction components. These interventions also had significant anti-inflammatory effects, as both the BE and Cur diets blocked recruitment of CD3$^+$ T cells and F4/80$^+$ macrophages to the submucosal and mucosal regions of *C. rodentium*-infected and DBZ-treated mice compared to the case in untreated controls (Fig. 7F and G).

DISCUSSION

Utilizing the TMCH model, the interplay between the Notch and Wnt/β-catenin pathways was examined in various genetic strains *in vivo*. Our study provides circumstantial evidence that in addition to the Wnt/β-catenin pathway, Notch signaling is also activated during TMCH and may work in tandem with the Wnt/β-catenin pathway to regulate hyperplasia and/or colitis following *C. rodentium* infection. We (23, 24, 28) and others (7, 14) have shown that activation of the Wnt/β-catenin pathway in the gut in response to bacterial infection is not unprecedented. However, neither the mechanism nor the consequence of aberrant regulation of the Notch pathway, either alone or in conjunction with Wnt/β-catenin signaling, is clearly understood. The cross talk between the Wnt and Notch pathways, including physical binding of Notch to β-catenin, has been described previously (21). In mammalian cells, GSK-3β directly phosphorylates the Notch protein, while β-catenin activates Jagged-1 transcription, thereby leading to the activation of the Notch pathway (21, 32). During tumorigenesis, both the Notch and Wnt pathways have been implicated in the regulation of β-catenin expression and function (9). These studies suggest that accurate coordination of the Notch and Wnt signals is indispensable for maintenance of intestinal homeostasis and that aberrant regulation of the cross talk may result in pathologies such as colitis or tumorigenesis. In the current study, while acute inhibition of the Notch pathway did not adversely affect the proliferative capacity of the colonic crypts, chronic inhibition of the Notch pathway not only affected crypt regeneration but also severely compromised barrier function in the colon, resulting in colitis. Recent studies have shown that epithelial cell-specific Notch signaling plays an essential role in the maintenance of gut homeostasis and in containment of intestinal inflammation (17). Similarly, Okamoto et al. (18) recently demonstrated that inhibition of Notch activation *in vivo* by use of a γ-secretase inhibitor (LY411575) resulted in severe exacerbation of inflammation when the agent was administered during the healing phase of dextran sodium sulfate (DSS)-induced colitis. Thus, either the onset or severity of colitis may be directly attributable to the loss of regenerative capacity of the colonic crypt owing to significant blockade of the Notch and Wnt/β-catenin pathways. Since blocking Notch signaling can affect the differentiation processes in the gut, we next examined the sequence of events associated with the onset of colitis in response to *C. rodentium* plus DBZ. The luminal mucus layer encompassing the gastrointestinal tract provides protection against commensal and/or pathogenic bacteria due to secretory products of intestinal goblet cells (e.g., the mucin glycoprotein Muc-2). Colonization by commensal intestinal microbiota is limited to an outer, "loose" mucus layer which provides the platform for interaction with the diverse oligosaccharides of mucin glycoproteins, whereas an "inner" adherent mucus layer is largely devoid of bacteria (13). Defective mucus layers resulting from a lack of Muc-2 mucin result in increased bacterial adhesion to the surface epithelium, increased intestinal permeability, and enhanced susceptibility to colitis caused by DSS (15). In the current study, we also observed a significant loss of the inner mucus layer in Carnoy's fixative-treated, paraffin-embedded sections prepared from *C. rodentium*-infected and DBZ-treated NIH:Swiss mice (Fig. 4E, panel i). Since in addition to DSS the barrier can be overcome by the parasite *Entamoeba histolytica* through the secretion of proteases that disrupt the integrity of the inner mucus layer, facilitating access to the underlying epithelium (12), it is tempting to speculate that loss or changes in the composition of the mucinous gel layer in *C. rodentium*-infected and DBZ-treated mice may have precluded the luminal anchor for bacteria, resulting in defects in the physical barrier. Indeed, disruption in the expression of tight junction proteins such as claudins and zonula occludens in the crypts from *C. rodentium*-infected and DBZ-treated mice correlated with increases in paracellular permeability leading to bacterial dissemination to distant organs. Thus, despite goblet cell metaplasia and an outflow of mucin, particularly in the crypts of *C. rodentium*-infected and DBZ-treated mice, these mice developed colitis. These findings are not unprecedented, however; in fact, recent studies have shown that mucus hypersecretion following deletion of the gene encoding protein O-fucosyl-transferase 1 (*Pofut1*), an enzyme required for Notch ligand binding, causes alteration of the mucus-associated flora, leading to enterocolitis (10). Similarly, disruption of the microbiota with the antibiotic metronidazole causes increased inflammation, altered goblet cell function, and thinning of the inner mucus layer, resulting in exacerbation of *C. rodentium*-induced colitis (35). Interestingly, infection of core-3$^{-/-}$ mice, which are defective in mucin secretion, with *C. rodentium* disrupted the intestinal barrier and induced colitis which was exacerbated following DBZ administration. The lack of crypt regeneration during *C. rodentium*- and DBZ-induced colitis in either NIH:Swiss or core-3$^{-/-}$ mice was not due to reallocation of colonic stem cells into goblet cells, as staining for the putative stem cell marker DCLK1 in samples from

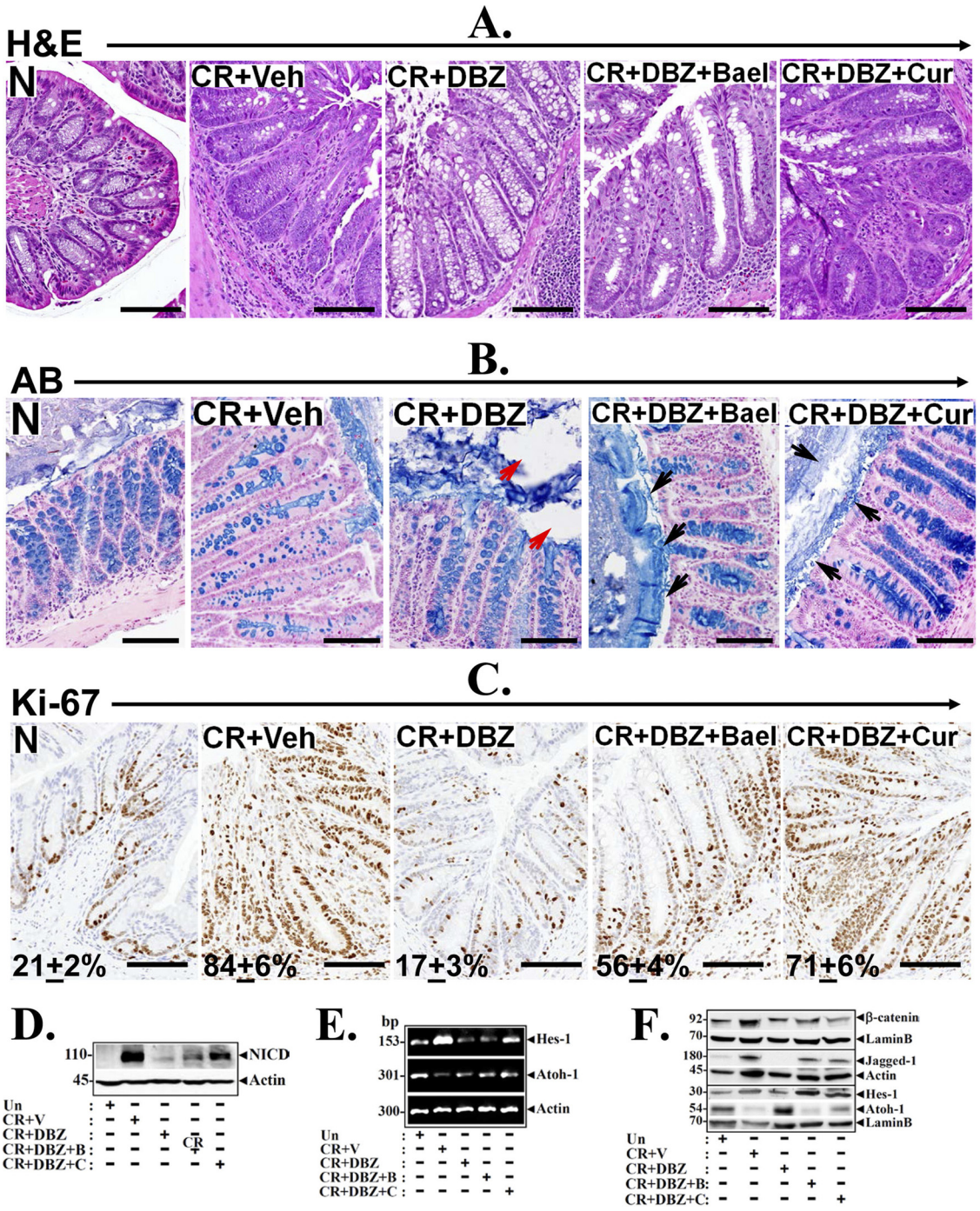

FIG 6 Effects of dietary bael extract and curcumin on Notch/Wnt signaling and crypt regeneration/hyperplasia. Uninfected normal (N) NIH:Swiss mice were infected with *C. rodentium* and received vehicle (CR+Veh), DBZ (CR+DBZ), DBZ plus bael extract (CR+DBZ+Bael), or DBZ plus curcumin (CR+DBZ+Cur), followed by euthanasia on day 12. Paraffin-embedded sections were analyzed by H&E (A), Alcian blue (AB) (B), and Ki-67 (C) staining (numbers represent percentages of cells positive for Ki-67). Red arrows, disrupted mucus layer in sections from *C. rodentium*-infected and DBZ-treated mice; black arrows, restoration of the inner mucus layer. Bars = 125 μm; $n = 3$ independent experiments. (D) Relative levels of NICD in the colonic crypts of uninfected normal mice (Un), *C. rodentium*-infected and vehicle-treated mice, *C. rodentium*-infected and DBZ-treated mice, *C. rodentium*-infected and DBZ-treated mice fed bael extract (B), and *C. rodentium*-infected and DBZ-treated mice fed curcumin (C). (E) RT-PCR analysis of total colonic crypt RNA samples for the indicated gene products. (F) Western blots showing crypt cellular/nuclear levels of β-catenin, Jagged-1, Hes-1, and Math-1. $n = 3$ independent experiments.

C. rodentium-infected and DBZ-treated mice was similar to that recorded for untreated *C. rodentium*-infected mice. Thus, while more studies are needed to understand the pathogenesis of colitis in response to *C. rodentium* plus DBZ, the abrogation of both Notch and Wnt/β-catenin signaling in core-3$^{-/-}$ mice, similar to that recorded in NIH:Swiss mice (Fig. 4 and 5), clearly suggests that controlled signaling via the Notch and Wnt/β-catenin pathways is probably indispensable for both proliferation and differ-

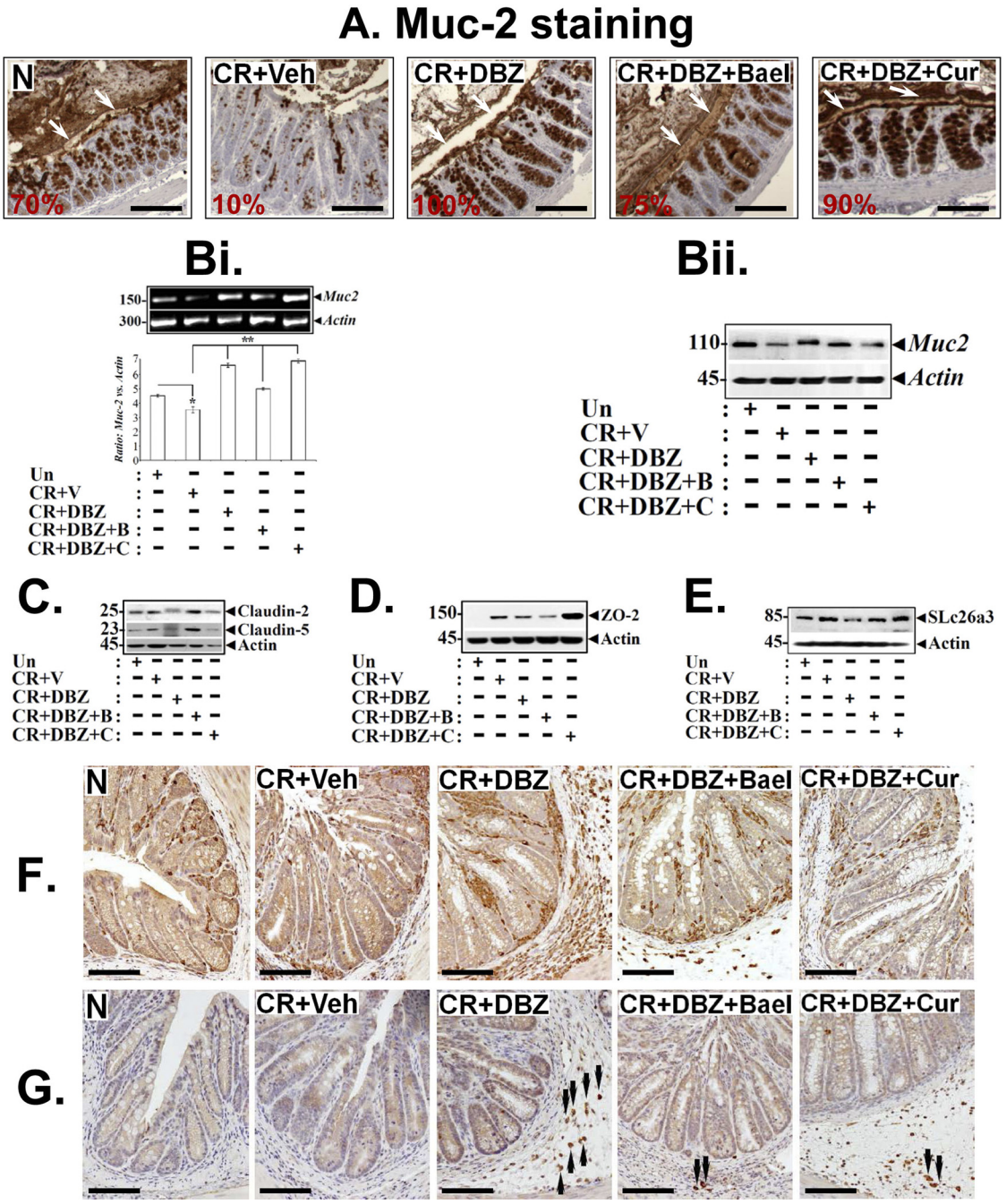

FIG 7 Effect of dietary intervention on replenishment of luminal mucus layers and recruitment of inflammatory cells. (A) Paraffin-embedded sections prepared from the distal colons of uninfected normal NIH:Swiss mice (N), *C. rodentium*-infected and vehicle-treated mice (CR+Veh), *C. rodentium*-infected and DBZ-treated mice (CR+DBZ), *C. rodentium*-infected and DBZ-plus-Bael-treated mice (CR+DBZ+Bael), and *C. rodentium*-infected and DBZ-plus-curcumin-treated mice (CR+DBZ+Cur) were stained with antibody for Muc-2. Numbers represent percentages of crypt positivity for Muc-2. Arrows point toward the inner mucus layer. Magnification, ×10. $n = 3$ independent experiments. (Bi) Total RNAs were extracted from the colonic crypts isolated from the above group of animals, and the indicated gene products were amplified by semiquantitative RT-PCR. A representative bar graph shows the ratio of Muc-2 to actin. *, $P < 0.05$ versus controls; **, $P < 0.05$ versus *C. rodentium*-infected mice; $n = 3$ independent experiments. (Bii) Western blots showing Muc-2 protein levels in the group of mice described for panel A. (C to E) Western blots showing relative levels of tight junction proteins claudin-2 and [hyphen]5 (C), ZO-2 (D), and SLC26A3 (E) in the group of mice described for panel A. (F and G) Paraffin-embedded sections prepared from the distal colons of NIH:Swiss mice after the indicated treatments were stained with antibody for CD3 (F) or F4/80 (G). Arrows in panel G indicate macrophage labeling. Bars = 50 μm; $n = 3$ independent experiments.

entiation processes associated with the maintenance of the barrier functions in the colon.

In terms of targeting the Wnt and Notch pathways, it has been difficult to block Wnt signaling *in vivo* given the nature of the signaling cascade downstream of APC. Similarly, systemic use of the six subgroups of γ-secretase inhibitors is associated with various adverse effects. We have shown in the past that TMCH is diet sensitive (5, 26) and that it is possible to distinctly separate the

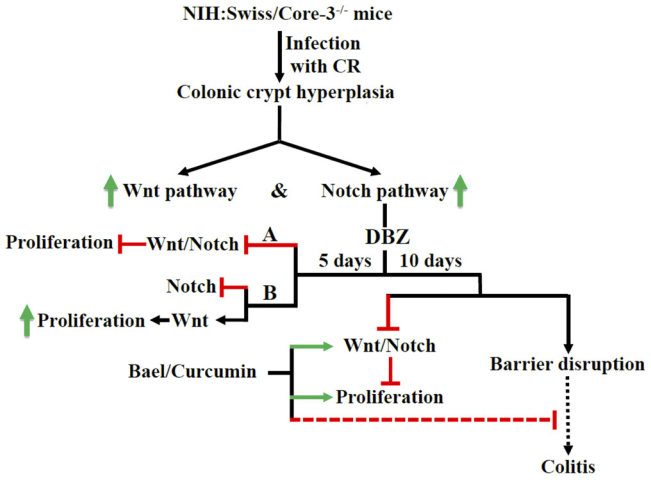

FIG 8 Proposed mechanism. Infection of either NIH:Swiss or core-3$^{-/-}$ mice with *C. rodentium* leads to colonic crypt hyperplasia which is associated with activation of both the Wnt/β-catenin and Notch pathways. Acute blockade of Notch signaling via DBZ before the onset of *C. rodentium*-induced crypt cell proliferation (A) also inhibits the Wnt/β-catenin pathway, leading to abrogation of hyperplasia. Late blocking after the onset of *C. rodentium*-induced crypt cell hyperproliferation fails to inhibit either the Wnt/β-catenin pathway or crypt hyperplasia (B). Chronic inhibition of the Notch pathway leads to an inability of the mucosa to regenerate, and along with defects in barrier function, it may trigger colitis (dotted lines). Dietary intervention with either bael or curcumin restores signaling via the two pathways, which may be associated with a restoration of barrier function and amelioration of colitis (dotted lines).

proproliferation properties of various dietary interventions from anti-inflammatory effects by using the TMCH model (6). Corroborating these studies, we found that both bael and curcumin diets had potent anti-inflammatory effects on *C. rodentium*- and DBZ-induced colitis and modulated the Notch signaling components to a greater extent than that for Wnt, indicating that modulation of Notch signaling may be more effective in reversing the outcome of colitis. Specifically, dietary intervention was associated with (i) restoration of NICD, Hes-1, and Jagged-1 expression in the crypts from *C. rodentium*-infected and DBZ-treated mice; (ii) replenishment of the inner mucus layer; and (iii) significant increases in tight junction protein expression in crypts from treated mice. In addition, we examined SLC26A3, an anion transporter which was recently implicated in the maintenance of the alkaline mucus layer and whose loss results in barrier impairment and mucosal inflammation in mice (4, 36). During *C. rodentium*- and DBZ-induced colitis, we observed a significant decrease in SLC26A3 expression in the crypts compared to that in untreated *C. rodentium*-infected mice, while dietary bael and curcumin resulted in a remarkable recovery in terms of restoring the expression of SLC26A3 in the crypts from treated mice. These studies provide evidence that intervention via dietary bael or curcumin results in (i) restoration of the inner mucus layer, based on Muc-2 staining; and (ii) restoration of the anion transporter SLC26A3, which may be associated with the establishment of an alkaline mucus layer in the lumen. These events, in conjunction with the repair of the tight junction machinery, may eventually ameliorate colitis in *C. rodentium*-infected and DBZ-treated mice. In conclusion, we believe that the balancing act between cell proliferation (via active Notch/Wnt signaling) and mucus production (via restoration of the Notch pathway) may facilitate crypt regeneration and restore barrier integrity, leading to amelioration of colitis during TMCH. Figure 8 represents a proposed model depicting the sequence of events related to hyperplasia and/or colitis following *C. rodentium* and *C. rodentium*-plus-DBZ interventions. Thus, the TMCH model provides an excellent template for examining the complex interplay between the Notch and Wnt/β-catenin pathways, and future studies will reveal in more detail the mechanisms by which their cross talk contributes to the physiological process of self-renewal as well as to the regeneration process after injuries to the gut epithelium.

ACKNOWLEDGMENTS

This work was supported by National Institutes of Health grant R01 CA131413 (to S.U.) and by start-up funds from the University of Kansas Medical Center, Kansas City, KS.

REFERENCES

1. **An G, et al.** 2007. Increased susceptibility to colitis and colorectal tumors in mice lacking core 3-derived O-glycans. J. Exp. Med. **204**:1417–1429.
2. **Barthold SW, Coleman GL, Bhatt PN, Osbaldiston GW, Jonas AM.** 1976. The etiology of transmissible murine colonic hyperplasia. Lab. Anim. Sci. **26**:889–894.
3. **Borenshtein D, Nambiar PR, Groff EB, Fox JG, Schauer DB.** 2007. Development of fatal colitis in FVB mice infected with Citrobacter rodentium. Infect. Immun. **75**:3271–3281.
4. **Borenshtein D, et al.** 2009. Decreased expression of colonic Slc26a3 and carbonic anhydrase IV as a cause of fatal infectious diarrhea in mice. Infect. Immun. **77**:3639–3650.
5. **Chandrakesan P, et al.** 2010. Novel changes in NF-κB activity during progression and regression phases of hyperplasia: role of MEK, ERK and p38. J. Biol. Chem. **285**:33485–33498.
6. **Chandrakesan P, et al.** 2012. Distinct compartmentalization of NF-κB activity in crypt and crypt-denuded lamina propria precedes and accompanies hyperplasia and/or colitis following bacterial infection. Infect. Immun. **80**:753–767.
7. **Duan Y, et al.** 2007. Beta-catenin activity negatively regulates bacteria-induced inflammation. Lab. Invest. **87**:613–624.
8. **Fortini ME, Artavanis-Tsakonas S.** 1994. The suppressor of hairless protein participates in notch receptor signaling. Cell **79**:273–282.
9. **Fre S, et al.** 2009. Notch and Wnt signals cooperatively control cell proliferation and tumorigenesis in the intestine. Proc. Natl. Acad. Sci. U. S. A. **106**:6309–6314.
10. **Guilmeau S, et al.** 2008. Intestinal deletion of protein O-fucosyltransferase in the mouse inhibits Notch signaling and causes enterocolitis. Gastroenterology **135**:849–860.
11. **Johansson ME, et al.** 2008. The inner of the two Muc2 mucin-dependent mucus layers in colon is devoid of bacteria. Proc. Natl. Acad. Sci. U. S. A. **105**:15064–15069.
12. **Lidell ME, Moncada DM, Chadee K, Hansson GC.** 2006. Entamoeba histolytica cysteine proteases cleave the MUC2 mucin in its C-terminal domain and dissolve the protective colonic mucus gel. Proc. Natl. Acad. Sci. U. S. A. **103**:9298–9303.
13. **Lievin-Le Moal V, Servin AL.** 2006. The front line of enteric host defense against unwelcome intrusion of harmful microorganisms: mucins, antimicrobial peptides, and microbiota. Clin. Microbiol. Rev. **19**:315–337.
14. **Liu X, Lu R, Wu S, Sun J.** 2010. Salmonella regulation of intestinal stem cells through the Wnt/beta-catenin pathway. FEBS Lett. **584**:911–916.
15. **McGuckin MA, Eri R, Simms LA, Florin TH, Radford-Smith G.** 2009. Intestinal barrier dysfunction in inflammatory bowel diseases. Inflamm. Bowel Dis. **15**:100–113.
16. **Napolitano LM, Koruda MJ, Meyer AA, Baker CC.** 1996. The impact of femur fracture with associated soft tissue injury on immune function and intestinal permeability. Shock **5**:202–207.
17. **Obata Y, et al.** 2012. Epithelial cell-intrinsic notch signaling plays an essential role in the maintenance of gut immune homeostasis. J. Immunol. **188**:2427–2436.
18. **Okamoto R, et al.** 2009. Requirement of Notch activation during regeneration of the intestinal epithelia. Am. J. Physiol. Gastrointest. Liver Physiol. **296**:G23–G35.
19. **Podolsky DK.** 2002. The current future understanding of inflammatory bowel disease. Best Pract. Res. Clin. Gastroenterol. **16**:933–943.

20. **Pullan RD, et al.** 1994. Thickness of adherent mucus gel on colonic mucosa in humans and its relevance to colitis. Gut **35**:353–359.
21. **Rodilla V, et al.** 2009. Jagged1 is the pathological link between Wnt and Notch pathways in colorectal cancer. Proc. Natl. Acad. Sci. U. S. A. **106**: 6315–6320.
22. **Roth GN, Chandra A, Nair MG.** 1998. Novel bioactivities of Curcuma longa constituents. J. Nat. Prod. **61**:542–545.
23. **Sellin JH, Umar S, Xiao J, Morris AP.** 2001. Increased beta-catenin expression and nuclear translocation accompany cellular hyperproliferation in vivo. Cancer Res. **61**:2899–2906.
24. **Sellin JH, Wang Y, Singh P, Umar S.** 2009. β-Catenin stabilization imparts progenitor phenotype to hyperproliferating colonic epithelia. Exp. Cell Res. **315**:97–109.
25. **Subramaniam D, et al.** 2008. Activation of apoptosis by 1-hydroxy-5,7-dimethoxy-2-naphthalene-carboxaldehyde, a novel compound from Agle marmelos. Cancer Res. **68**:1–9.
26. **Umar S, Morris AP, Kourouma F, Sellin JH.** 2003. Dietary pectin and calcium inhibit colonic proliferation in vivo by differing mechanisms. Cell Prolif. **36**:361–375.
27. **Umar S, Sarkar S, Wang Y, Singh P.** 2009. Functional cross-talk between beta-catenin and NF-KappaB signaling pathways in colonic crypts of mice in response to progastrin. J. Biol. Chem. **284**:22274–22284.
28. **Umar S, Wang Y, Morris AP, Sellin JH.** 2007. Dual alterations in casein kinase I-epsilon and GSK-3beta modulate beta-catenin stability in hyperproliferating colonic epithelia. Am. J. Physiol. Gastrointest. Liver Physiol. **292**:G599–G607.
29. **Umar S.** 2010. Intestinal stem cells. Curr. Gastroenterol. Rep. **12**:340–348.
30. **Vallance BA, Deng W, Knodler LA, Finlay BB.** 2002. Mice lacking T and B lymphocytes develop transient colitis and crypt hyperplasia yet suffer impaired bacterial clearance during *Citrobacter rodentium* infection. Infect. Immun. **70**:2070–2081.
31. **van de Wetering M, et al.** 2002. The beta-catenin/TCF-4 complex imposes a crypt progenitor phenotype on colorectal cancer cells. Cell **111**: 241–250.
32. **van Es JH, Clevers H.** 2005. Notch and Wnt inhibitors as potential new drugs for intestinal neoplastic disease. Trends Mol. Med. **11**:496–502.
33. **van Es JH, et al.** 2005. Notch/gamma-secretase inhibition turns proliferative cells in intestinal crypts and adenomas into goblet cells. Nature **435**: 959–963.
34. **Wang Y, Xiang GS, Kourouma F, Umar S.** 2006. Citrobacter rodentium-induced NF-kappaB activation in hyperproliferating colonic epithelia: role of p65 (Ser536) phosphorylation. Br. J. Pharmacol. **148**:814–824.
35. **Wlodarska M, et al.** 2011. Antibiotic treatment alters the colonic mucus layer and predisposes the host to exacerbated Citrobacter rodentium-induced colitis. Infect. Immun. **79**:1536–1545.
36. **Xiao F, et al.** 2012. Colonic Slc26A3 establishes alkaline mucus layer and its loss results in barrier impairment and mucosal inflammation in mice. Gastroenterology **5**(Suppl 1):S-74.